FEBS Letters

FEBS PRESS science publishing by scientists

Interaction of replication protein A with two acidic peptides from human Bloom syndrome protein

Donguk Kang[1,†], Sungjin Lee[1,†], Kyoung-Seok Ryu[2], Hae-Kap Cheong[2], Eun-Hee Kim[2] and Chin-Ju Park[1]

1 Department of Chemistry, Gwangju Institute of Science and Technology, Gwangju, Korea
2 Division of Magnetic Resonance, KBSI, Chungbuk, Korea

Correspondence
C.-J. Park, Department of Chemistry, Gwangju Institute of Science and Technology, Gwangju 61005, Korea
Fax: + 82 62 715 2866
Tel: + 82 62 715 3630
E-mail: cjpark@gist.ac.kr

†These authors contributed equally to this work

(Received 19 July 2017, revised 9 January 2018, accepted 24 January 2018, available online 15 February 2018)

doi:10.1002/1873-3468.12992

Edited by Christian Griesinger

Bloom syndrome protein (BLM) is one of five human RecQ helicases which maintain genomic stability. Interaction of BLM with replication protein A (RPA) stimulates the DNA unwinding ability of BLM. The interaction is expected to be crucial in the DNA damage response. Although this stimulation of BLM by RPA is of particular importance in cancer cells, the precise binding surfaces of both proteins are not well understood. In this study, we show by fluorescence polarisation anisotropy that both acidic surface peptides of BLM specifically bind to the RPA70N domain of RPA. Our NMR analysis and docking models show that the basic cleft region of RPA70N is the binding site for both peptides and that the acidic peptide/basic cleft interaction governs RPA-BLM binding.

Keywords: BLM; Bloom syndrome; NMR; protein-protein interaction; replication protein A

Replication protein A (RPA) is the eukaryotic single-stranded (ss) DNA-binding protein involved in DNA metabolism functions such as replication, repair, and recombination [1–3]. Human RPA consists of three subunits: RPA70, RPA32 and RPA14 (Fig. 1A). RPA is a modular protein and contains 6 oligonucleotide binding (OB) folds. Among these OB-folds, DNA binding domains (DBDs) A, B and C (in RPA70) and DBD-D (in RPA32) function as the main ssDBDs [4,5]. DBD-F in the N-terminal part of RPA70 (RPA70N) is known to be involved in protein-protein interactions with various DNA damage response proteins such as ATRIP, RAD9, MRE11 and p53 [6,7]. Recently, it has been revealed that large T antigen, a helicase protein of Simian virus 40 (SV40), human DNA helicase B, and Ewing tumour-associated antigen 1 (ETAA1) also physically interact with human RPA70N [8–10]. In each case, the basic cleft of RPA70N between loops L12 and L45 is the binding surface for acidic surface peptides (Fig. 1B).

Bloom syndrome protein (BLM), 1 of 5 human RecQ helicases, contributes to genomic stability via its helicase activity [11,12]. It has been revealed that BLM physically and functionally interacts with RPA, and the N-terminal segment of BLM (1–447) was identified as the binding region for RPA [13] (Fig. 1A). Conversely, the BLM binding region of RPA was generally identified as RPA70 [13,14]. Interestingly, a BLM helicase construct which lacked the RPA interaction site showed reduced unwinding activity for long DNA substrates [13]. Also, a single-molecule Förster resonance energy transfer study showed that RPA promotes the reinitiation of stalled DNA unwinding by BLM helicase [15]. These findings imply that the direct

Abbreviations
BLM, Bloom syndrome protein; DBD, DNA binding domain; FITC, fluorescein isothiocyanate; FPA, fluorescence polarisation anisotropy; OB, oligonucleotide binding; RPA, replication protein A.

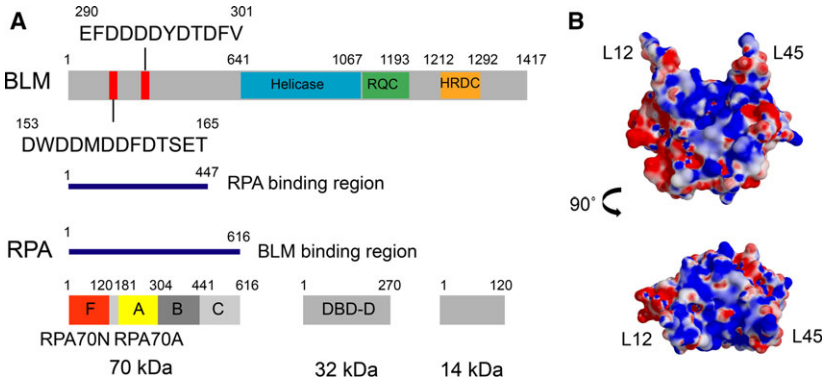

Fig. 1. (A) Domain structure of human BLM and RPA. The amino acid sequences of the two BLM peptides ($BLM_{153–165}$ and $BLM_{290–301}$) tested in this study are shown and their positions in the sequence indicated in red. Previously defined BLM and RPA binding regions are marked. (B) The electrostatic surface of RPA70N is shown. Electrostatics calculations were performed with PDB2PQR [36] and visualised with PyMOL [27]. Positively charged (+8 kT/e in blue) and negatively charged (−8 kT/e in red) amino acids are marked.

BLM-RPA interaction is essential for the stimulation by RPA of helicase-catalysed DNA unwinding. In particular, it is known that Sgs1, the yeast homologue of BLM, interacts with Rpa70 in yeast and has a crucial role in checkpoint signaling by recruiting Rad53 to regions of ssDNA at stalled replication forks [16]. BLM is expected to have a similar role in human cells by interacting with RPA [17]. Considering the importance of checkpoint signaling in cancer cells, it is necessary to understand the details of the BLM-RPA interaction for developing novel anticancer strategies.

Previous research showed that the acidic region of Werner syndrome protein (WRN), another human RecQ helicase, is essential for its interaction with RPA [13]. By analogy to the WRN-RPA interaction, it has been suggested that the acidic surface peptides of BLM are crucial for its binding to RPA70 [13]. Based on these findings, and considering sequences of other RPA-interacting proteins such as ATRIP, MRE11, and p53, we chose two acidic surface peptides in the N-terminal region of BLM for examining its binding to RPA: 153–165 (DWDDMDDFDTSET) and 290–301 (EFDDDDYDTDFV). Conversely, RPA70N is the primary candidate for BLM binding, because it is involved in various protein-protein interactions as described above. We also assessed the RPA70A domain as a potential BLM binding site, because this region is necessary for WRN binding [13,18].

To investigate the RPA-BLM interaction in detail, we analysed the chemical shift perturbations in RPA70N and RPA70A during titration with the BLM peptides. We found that both peptides specifically bound to RPA70N, but not RPA70A. We mapped the binding surfaces of the BLM peptides on RPA70N and also determined the dissociation constants for both peptides using fluorescence polarisation anisotropy (FPA). Our analysis and docking models provide detailed information about the BLM-RPA interaction and give insights into the common acidic peptide-basic cleft interaction mediated by RPA70N.

Materials and methods

Sample preparation

The fluorescein isothiocyanate (FITC)-labelled $BLM_{153–165}$ (FITC-aca-DWDDMDDFDTSET) and $BLM_{290–301}$ (FITC–aca-EFDDDDYDTDFV) peptides were purchased from AnyGen (Gwangju, Korea). The FITC-$BLM_{153–165}$ and FITC-$BLM_{290–301}$ peptides were purified using HPLC to 97.5% and 95.4% purity respectively. Unlabelled $BLM_{153–165}$ and $BLM_{290–301}$ were also purchased from AnyGen and purified with the same method. RPA70N (residues 1–120) and RPA70A (residues 181–304) constructs were cloned into a pET15b vector and transformed into BL21(DE3) cells. The proteins were overexpressed and purified as described previously [19,20]. ^{15}N-labelled proteins were obtained by growing cells in M9 media containing $^{15}NH_4Cl$ and unlabelled D-glucose.

NMR experiments

^{1}H-^{15}N HSQC experiments were performed using a Bruker 900 MHz NMR spectrometer equipped with a cryogenic probe (KBSI, Ochang). ^{15}N-labelled RPA70N and RPA70A were prepared at 0.3 mM in 20 mM Tris, 100 mM NaCl, 2 mM DTT, pH 7.4. For BLM peptide titrations, $BLM_{153–165}$ was added at molar ratios of 0, 0.1, 0.15, 0.25, 0.5, 1.0 and $BLM_{290–301}$ was added at molar ratios of 0, 0.1, 0.25, 0.5, 1.0, 2.0. All experiments were performed at 298 K. Two-dimensional NMR data were processed with

the program Topspin and analysed with the program Sparky [21]. Averaged chemical shift perturbations ($\Delta\delta_{avg}$) were calculated with equation 1,

$$\Delta\delta_{avg} = \sqrt{(\Delta\delta_H)^2 + (\Delta\delta_N/5.88)^2} \quad (1)$$

where $\Delta\delta_H$ and $\Delta\delta_N$ are the chemical shift differences in the amide proton and nitrogen resonances, respectively. Residues which have $\Delta\delta_{avg}$ more than one or two standard deviations above the average are considered as significantly perturbed one. We used the amide chemical shifts of RPA70N and RPA70A that were published previously [22,23].

Fluorescence polarisation anisotropy experiments

We used FITC labels with 6-aminohexanoic acid spacer on the N-terminal of both peptides for fluorescence polarisation assays. FITC is widely used fluorescence dye and known to contribute partial negative charges at neutral pH. The effect of FITC labeling was previously tested with FITC labelled ATRIP peptides and RPA70N [20]. The study showed the labelled and unlabelled peptides have identical binding mode while the FITC labeling had a slightly higher binding affinity to RPA70N. On the basis of this, we thought that FITC labeling in our system does not severely alter the binding mode of peptides. In this study, increasing concentrations (0–200 μM) of RPA70N (or RPA70A) in 200 μL of assay buffer (50 mM HEPES, 100 mM NaCl, 2 mM DTT, pH 7.5) containing 5% DMSO and 50 nM FITC-BLM peptides were mixed on a shaker for 15 min and incubated for 1 h at room temperature. Corning 96-well black plates (Polystyrene, non-treated flat bottom) were used. The FPA intensities were measured at an excitation wavelength of 485 nm and an emission wavelength of 528 nm using the Cytation5 (BioTek, Gwangju, South Korea) and GEN5 software (GIST, Gwangju). The emission polarisation anisotropy was determined with reference to a previous report [20]. Emission anisotropy data were analysed using GRAPHPAD PRISM version 7.01 for Windows (GraphPad Software, La Jolla, CA, USA, www.graphpad.com). Anisotropy values were plotted against an *x*-axis of increasing concentrations of RPA70N or RPA70A, and a 'saturation one-site' fitting model was used to determine the dissociation constant (K_d). An FPA competition assay was performed to compare the interaction of RPA70N with FITC-$BLM_{153–165}$ with that of a known protein interaction inhibitor. We chose 3,3′,5,5′-tetraiodothyroacetic acid as the RPA70N inhibitor based on a previous report [20]. Increasing concentrations of 3,3′,5,5′-tetraiodothyroacetic acid (0–500 μM) were added to 6 μM of RPA70N and 500 nM of FITC-$BLM_{153–165}$ in 200 μL of assay buffer containing 5% DMSO. The contents were mixed on the shaker for 15 min and incubated for 1 h at room temperature. The IC_{50} value was determined using the log[Inhibitor] *vs.* response – Variable slope (four parameter) method in GraphPad Prism. The IC_{50} value was converted into a K_d value using the K_i calculator at http://sw16.im.med.umich.edu/software/calc_ki/ [24].

Docking

Modelling of the RPA70N-BLM peptide complexes was performed on the CABS-dock Web server [25]. We used the crystal structure of RPA70N (RCSB ID: 2B29) as the starting coordinates, and coordinates for the peptides were generated by the server based on each peptide sequence [7]. Fifty simulation cycles and default parameters were used for the modelling. After flexible docking (10 000 models generation) and initial filtering, the filtered 1000 models are grouped into clusters in the k-medoid clustering procedure. Detailed methods were described previously [26]. The highest cluster density model of each simulation was further analysed. The binding surface was defined as pairs of peptide/protein residues closer than 4.5 Å in the complex. The docked structures were visualised with Pymol [27]. To validate the docking simulation, we tested the same default parameters of CABS-dock simulation for RPA70N-$p53_{33–60}$ complex. Also we performed HADDOCK simulation for RPA70N-$BLM_{153–165}$ complex. HADDOCK requires binding sites (active residues) and the coordinates of the protein and the peptide. For the RPA70N side, R31, R43, S55, M57, A59, T60, N85, V93, Y118 and E120 were used as active residues based on the NMR data. For the $BLM_{153–165}$, two aromatic residues (W154 and F160) were chosen based on the binding affinity test of ATRIP peptides to RPA70N [28]. We used the crystal structure of RPA70N (RCSB ID: 2B29) as the starting coordinate and the coordinate of $BLM_{153–165}$ from model 1 of CABS-dock results. We used HADDOCK 2.2 web version (http://milou.science.uu.nl/services/HADDOCK2.2/) with the default setting [29]. Finally, we tested pep-ATTRACT server for both RPA70N-$BLM_{153–165}$ and RPA70N-$BLM_{290–301}$ complexes with the default setting (http://bioserv.rpbs.univ-paris-diderot.fr/services/pepATTRACT/) [30].

Results

Chemical shift perturbation of RPA70N upon binding to BLM peptides

Figure 2A shows the averaged chemical shift perturbations ($\Delta\delta_{avg}$) of RPA70N upon binding to $BLM_{153–165}$. Although the chemical shift change values were small ($\Delta\delta_{avg} \leq 0.16$), significant chemical shift changes were specifically observed in residues in the basic cleft region (β1, L12, β2, β3 and L45) and the C-terminal region of RPA70N. Among those, ^1H-^{15}N cross-peaks of R31, S55, R92 and E120 with increasing molar ratio of $BLM_{153–165}$ are shown in Fig. 2B.

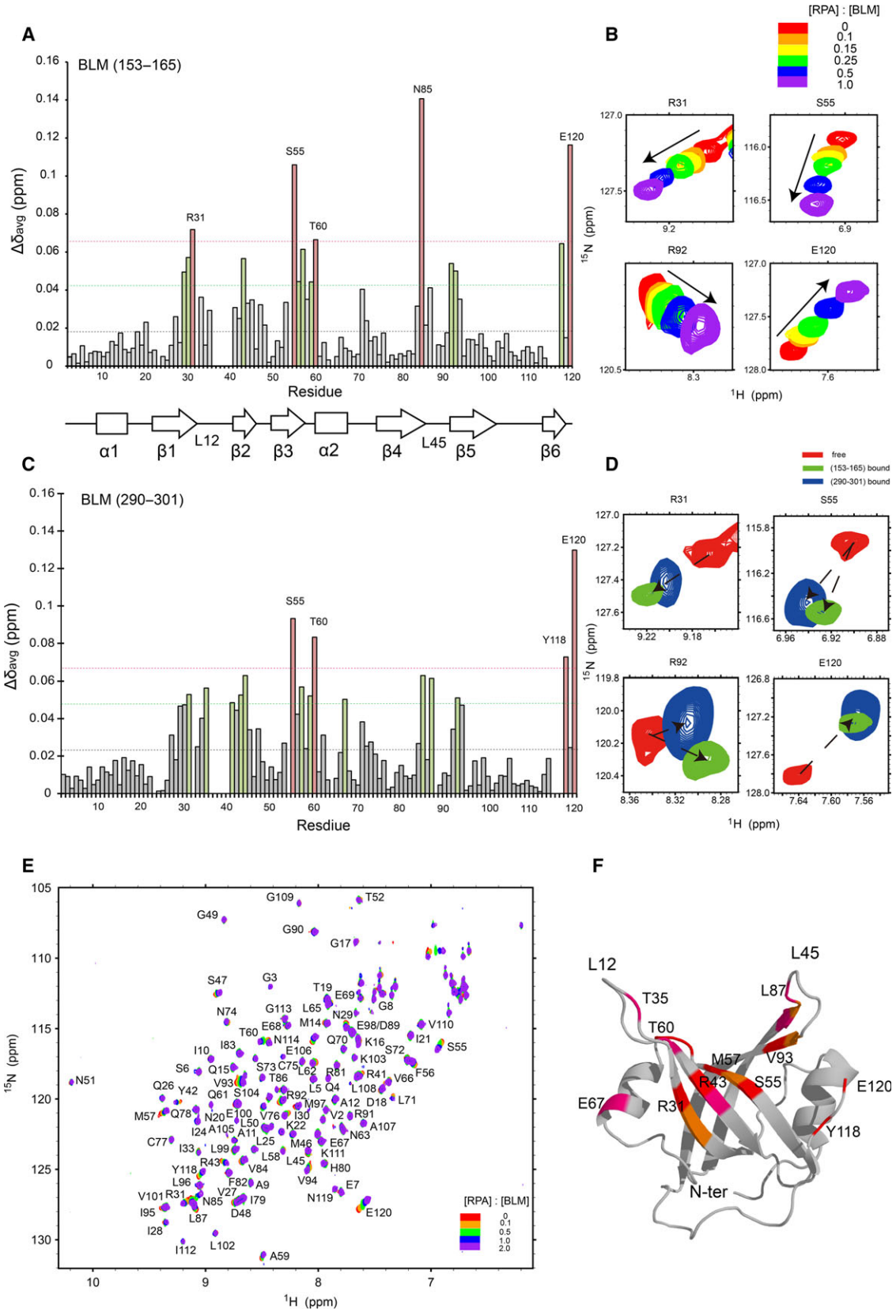

Fig. 2. Chemical shift perturbations in RPA70N upon interaction with BLM peptides. (A) Average chemical shift changes of RPA70N upon $BLM_{153–165}$ binding. Residues that have $\Delta\delta_{avg}$ over one standard deviations cutoff (green bar) and over two standard deviations cutoff (red bar) are marked. (B) ^{1}H-^{15}N cross-peaks of R31, S55, R92 and E120 of RPA70N upon titration with $BLM_{153–165}$. (C) Average chemical shift changes of RPA70N upon $BLM_{290–301}$ binding. Residues that have $\Delta\delta_{avg}$ over one standard deviations cutoff (green bar) and over two standard deviations cutoff (red bar) are marked. (D) Overlaid ^{1}H-^{15}N cross-peaks of R31, S55, R92, and E120 of RPA70N in the free (red), $BLM_{153–165}$ bound (green), and $BLM_{290–301}$ bound forms. (E) ^{1}H-^{15}N HSQC spectral overlay of RPA70N upon the titration of $BLM_{290–301}$. (F) Residues significantly perturbed by $BLM_{153–165}$ and $BLM_{290–301}$ are mapped onto the crystal structure of RPA70N. Residues perturbed by both peptides are coloured in red. Residues perturbed by $BLM_{153–165}$ or $BLM_{290–301}$ are coloured in orange and pink, respectively. In (A) and (C), dashed lines indicate the average perturbation (black), one standard deviation over the average (green), and two standard deviations over the average (red).

$BLM_{290–301}$ titration also induced similar chemical shift changes in RPA70N (Fig. 2C). S55, T60, and E120 of RPA70N shifted more than two standard deviations above the average in the presence of both peptides. Interestingly, most of the shifted peaks except R92 showed the same direction of change with both peptides (Fig. 2D,E). The residues perturbed more than one standard deviation by both peptides (R31, R43, S55, M57, A59, T60, N85, V93, Y118 and E120) were used to map a common binding surface on the crystal structure of RPA70N [7] (Fig. 2F). This surface is the same as previously defined binding surfaces of RPA70N for p53 [7], ATRIP, RAD9, MRE11 [6], SV40 [8] and ETAA1 [10]. This implies that both BLM peptides use the same binding surface as other RPA70N-interacting proteins.

Chemical shift perturbation of RPA70A upon binding to BLM peptides

Figures 3A,B show the chemical shift changes of RPA70A upon addition of $BLM_{153–165}$ and $BLM_{290–301}$ respectively. Overall, the amplitudes of $\Delta\delta_{avg}$ were much smaller than in the case of RPA70N with BLM peptides. The maximum $\Delta\delta_{avg}$ was less than 0.06, while that of RPA70N was around 0.15. This implies that the binding of both peptides to RPA70A is weaker than the binding to RPA70N. Cross-peaks of N214, E290 and H293 showed relatively prominent chemical shift changes in the presence of both peptides. These residues are near the ssDNA-binding surface of RPA70A. However, magnitudes of $\Delta\delta_{avg}$ by ssDNA were significantly larger with a μM order of K_d [31]. It is expected that the binding affinity of the peptides is much weaker than that of ssDNA. This implies that both peptides have a binding preference for the RPA70N domain over the RPA70A domain.

Fluorescence polarisation anisotropy assays

Figure 4A shows the fluorescence anisotropy of the FITC-labelled BLM peptides in the presence of increasing concentrations of RPA70N. Via curve fitting, the K_d of the RPA70N-$BLM_{153–165}$ complex was determined to be 5.76 ± 0.86 μM, and the K_d of the RPA70N-$BLM_{290–301}$ complex was determined to be 13.5 ± 2.4 μM. The binding of the peptides to RPA70N produced a typical hyperbolic binding isotherm. In contrast, RPA70A did not specifically bind to either BLM peptide (Fig. 4B). The anisotropy values of both FITC-labelled peptides with increasing concentrations of RPA70A were not saturated and could not be fitted. This result is consistent with our NMR data, which showed that only RPA70N exhibited significant chemical shift changes upon titration of the BLM peptides.

Figure 4C shows the fluorescence anisotropy of FITC-$BLM_{153–165}$ in the presence of increasing concentrations of 3,3′,5,5′-tetraiodothyroacetic acid, which is known to inhibit RPA70N-ATRIP complex formation [20]. The decrease in anisotropy of FITC-$BLM_{153–165}$ at higher concentrations indicates that the inhibitor and the BLM peptide compete for the same binding surface on RPA70N. This result confirmed that FITC-$BLM_{153–165}$ interacts with RPA70N via the same binding surface as other RPA-interacting proteins. The IC_{50} value of the inhibitor was determined to be 40.63 ± 1.17 μM, and the K_d value was determined to be 17.77 ± 0.52 μM. These values were comparable to those published in a previous study [20].

Docking model of the RP70N-BLM peptide complex

To investigate the details of the RPA70N-BLM peptide binding surfaces, we performed docking simulations. The docking for the RPA70N-$BLM_{153–165}$ complex generated 10 clusters with a combined 1000 models. The details of structural clustering are shown in Table S1. The first cluster contained 114 structures with a 2.82 Å average cluster RMSD (an average pairwise Cα RMSD value between models grouped in a cluster). All the major clusters (number of elements ≥90, clusters 1 to 7) consist of structural models with

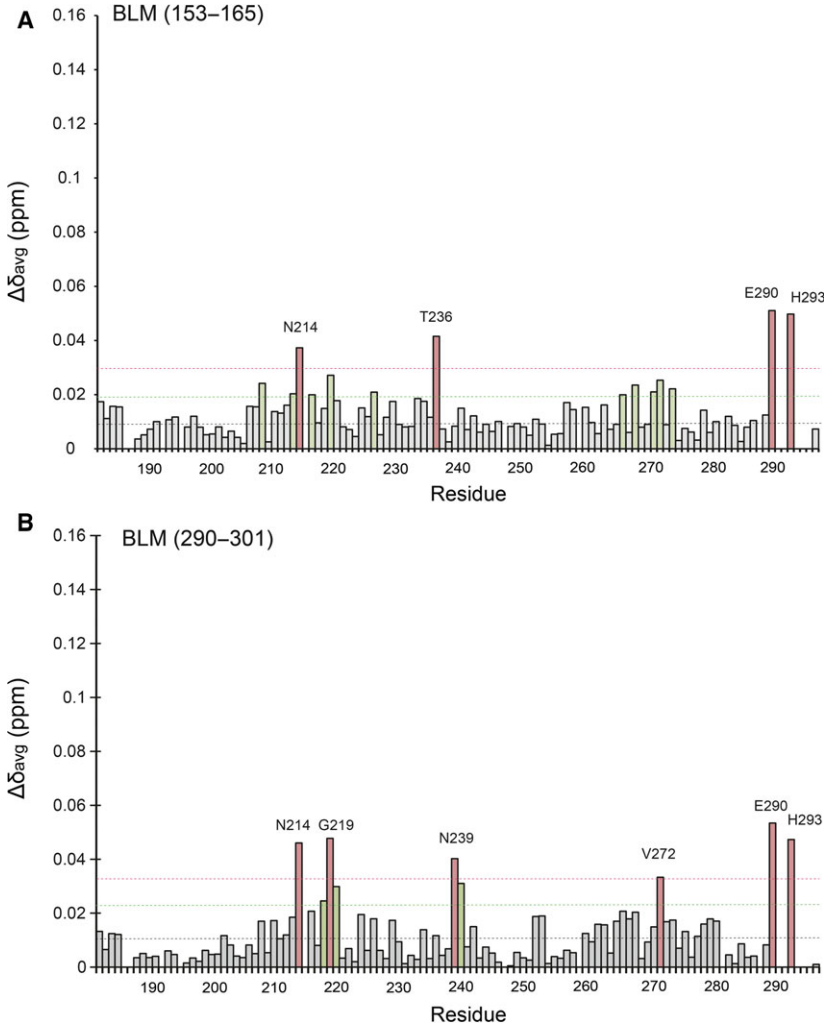

Fig. 3. Chemical shift perturbations in RPA70A upon interaction with BLM peptides. (A) Average chemical shift changes of RPA70A upon $BLM_{153–165}$ binding. (B) Average chemical shift changes of RPA70A upon $BLM_{290–301}$ binding. Residues that have $\Delta\delta_{avg}$ over the one standard deviation cutoff (green bar) and over the two standard deviations cutoff (red bar) are marked. The average perturbation (black), one standard deviation over the average (green), and two standard deviations over the average (red) are shown as dashed lines.

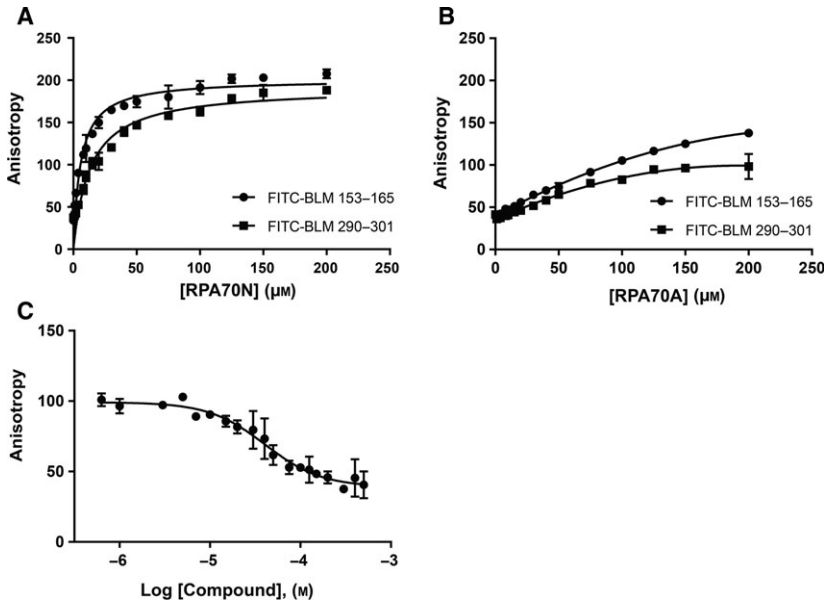

Fig. 4. Fluorescence polarisation anisotropy of BLM peptides upon addition of RPA domains. (A) Fluorescence polarisation anisotropy values of FITC-labelled BLM peptides upon titration with RPA70N. (B) Fluorescence polarisation anisotropy values of FITC-labelled BLM peptides upon titration with RPA70A. (C) Competitive inhibition of $FITC\text{-}BLM_{153–165}$ binding to RPA70N by 3,3′,5,5′-tetraiodothyroacetic acid.

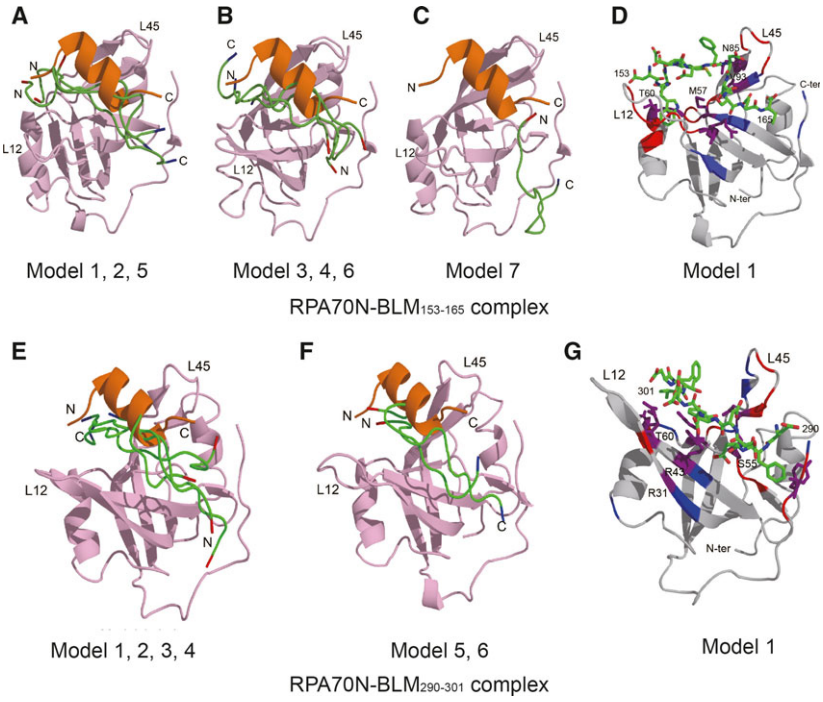

Fig. 5. Docking models of the (A–D) RPA70N–$BLM_{153–165}$ and (E–G) RPA70N–$BLM_{290–301}$ complexes. $BLM_{153–165}$ and $BLM_{290–301}$ are displayed in green. (A) Peptides of model 1, 2 and 5 are in the same orientation of modified ATRIP peptides (orange). (B) Peptides of model 3, 4 and 6 are in the opposite direction. (C) Model 7 peptide binds to a different area of RPA70N. (D, G) In model 1 of each complex, Residues perturbed by more than one standard deviation above the average in the NMR experiments and within 4.5 Å in the docking are coloured in purple. Residues that only have Δδ more than one standard deviation above the average are marked in blue. Residues with only a distance of ≤4.5 Å in the docking are marked in red. (E) Model 1, 2, 3 and 4 peptides are placed in the opposite direction to ATRIP peptide (orange). (F) Peptides of model 5 and 6 are in the same orientation.

an extended peptide conformation without any secondary structure. The predicted peptide binding site in six of the seven major clusters was the basic cleft region (Fig. 5A–C). However, the orientations of the bound peptides were mixed. In models 1, 2 and 5, the peptides were oriented parallel to the modified ATRIP peptide bound to RPA70N (RCSB ID: 4NB3, [28]) while the peptide orientation in models 3, 4 and 6 was reversed (Fig. 5A,B). In model 1, W154 of the $BLM_{153–165}$ peptide was in close proximity to P40, R41, Y52, M57, L58, A59, T60 and N63 of RPA70N. Basic residues of RPA70N (R41, R43, and R91) interacted with acidic residues of BLM peptides (D159 and E164). The binding interfaces of the complex are composed of residues with significant chemical shift changes ($\Delta\delta_{avg} \geq$ average + 1σ) and their neighbours (Fig. 5D).

Similar results were observed when modelling the RPA70N-$BLM_{290–301}$ complex. The details of structural clustering are shown in Table S2. The first cluster contained 149 structures with an average cluster RMSD of 2.98 Å. Like the $BLM_{153–165}$ peptide, this peptide was in an extended, unstructured conformation in the average complex structure of all major clusters (number of elements ≥ 100, clusters 1 to 6). The representative structures of each major cluster had the peptide binding to the basic cleft of RPA70N, while the binding orientations were mixed. Models 1, 2, 3 and 4 had the BLM peptide antiparallel to the modified ATRIP peptide bound to RPA70N (RCSB ID: 4NB3, [28]) (Fig. 5E). Models 5 and 6 had the BLM peptide in the same orientation as the modified ATRIP peptide (Fig. 5F). In model 1, most residues of $BLM_{290–301}$ were involved in RPA70N binding. Basic residues of RPA70N (R31, R41, R43, R91 and R92) were near to E290, D292, D294, D295 and D297 of BLM (Fig. 5G). Both BLM peptides passed through the two loops (L12 and L45) and had similar interactions with RPA70N (Fig. S1A). Detailed interactions per residue of both peptides are shown in Fig. S1B.

Validation of the docking simulation

To validate our docking simulation, we performed the CABS-dock running for RPA70N-$p53_{33–60}$ complex with default parameters. CABS-dock successfully predicted the secondary structure of $p53_{33–60}$ using PSIPRED. Two helices were correctly predicted (Fig. 6A). The final models also have at least one helical conformation. The details of structural clustering are shown in Table S3. We examined cluster 1 to 6. As shown in Fig. 6B–I, the main binding site of RPA70N are located in the basic cleft region. However, the helix conformation and orientation are various. Compared to experimentally known RPA70N-$p53_{33–60}$ structure, model 5 (Fig. 6G) is the best-matched one. Model 1 used the same binding interfaces with model 5, but its orientation of H2 is opposite. The data showed that

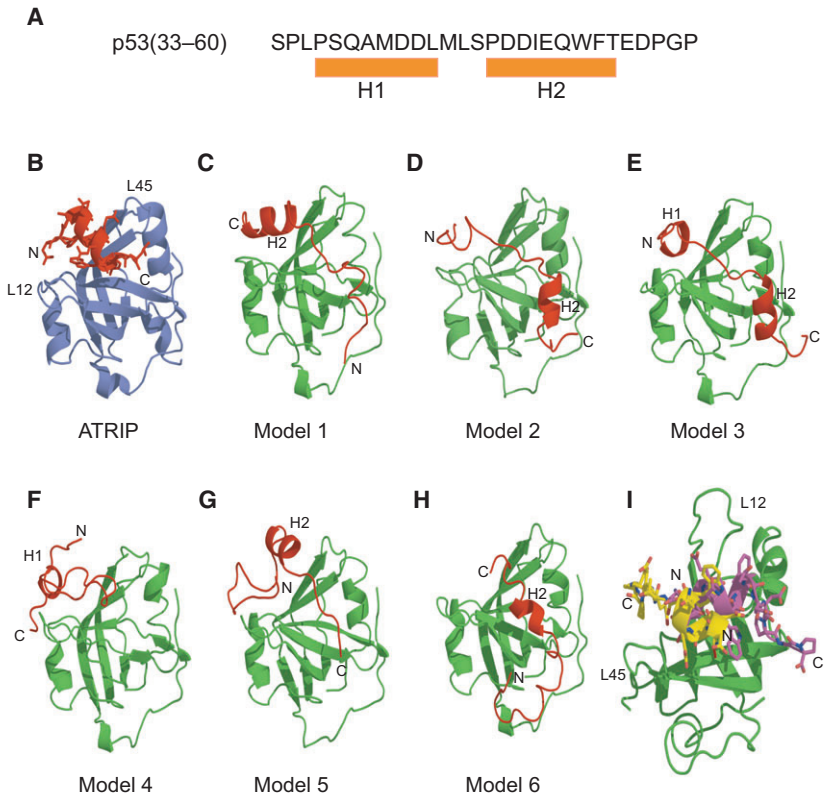

Fig. 6. (A) Primary sequence of $p53_{33–60}$ and predicted secondary structure by CABS-dock (B) Crystal structure of modified ATRIP peptide and RPA70N complex (RCSB ID: 4NB3). Docking models of (C–H) RPA70N-$p53_{33–60}$ complex from model 1 to 6. (I) Helix 2 of model 1 (yellow) and 5 (pink) are shown.

the CABS-dock could recover helical conformation without previous knowledge but the orientation could be mixed.

For RPA70N-$BLM_{153–165}$ complex, we also performed HADDOCK simulation. HADDOCK clustered 190 structures in four clusters, which represent 95.0% of the water-refined models HADDOCK generated. Except cluster 1 that has 169 structures, other three clusters have z-score as 0 and cluster sizes are 12, 5 and 4 respectively. Details of Cluster 1 are shown in Table S4. The four best structures of cluster 1 are shown in Fig. 7A,B. The peptide binding region is consistent with the basic cleft region, but orientations are not converged.

Finally, we tested pep-ATTRACT server for both complexes. The 50 lowest energy models of RPA70N-$BLM_{153–165}$ complex and RPA70N-$BLM_{290–301}$ complex are shown in Fig. 7C,D. The peptide conformations are all extended. The binding surfaces include the basic cleft region but the other areas are also predicted as the possible binding sites.

Discussion

In this study, we showed that two acidic segments (153–165 and 290–301) of the N-terminal domain of BLM specifically bind to RPA70N. Our NMR data indicate that residues in the basic cleft of RPA70N were perturbed by both peptides with similar magnitudes. Because RPA70 is a large protein with multiple domains, it is worth defining the RPA70N domain specifically as the BLM binding region. Interestingly, RPA70A, the major ssDNA binding domain, shares a common OB-fold with RPA70N, and Rad51, which contains several acidic amino acids, binds to RPA70A [32]. However, in our study, both BLM peptides showed a clear preference for binding RPA70N over RPA70A. This suggests that BLM can interact with RPA via the RPA70N domain while the other domains of RPA protect ssDNA. Stimulation of BLM activity by RPA may be mediated through this protein–protein interaction.

The surface of RPA70N to which BLM binds has multiple interaction partners, including DNA damage response proteins such as ATRIP and ETAA1 [6,10]. A sequence comparison of the two BLM peptides with the primary binding sites of other RPA-binding proteins confirmed that those sequences commonly have high acidic content and include several hydrophobic residues (Fig. 8). It is known that F55 of ATRIP is critical for RPA binding [28]. In the BLM peptides, W154 of $BLM_{153–165}$ and F291 of $BLM_{290–301}$ are

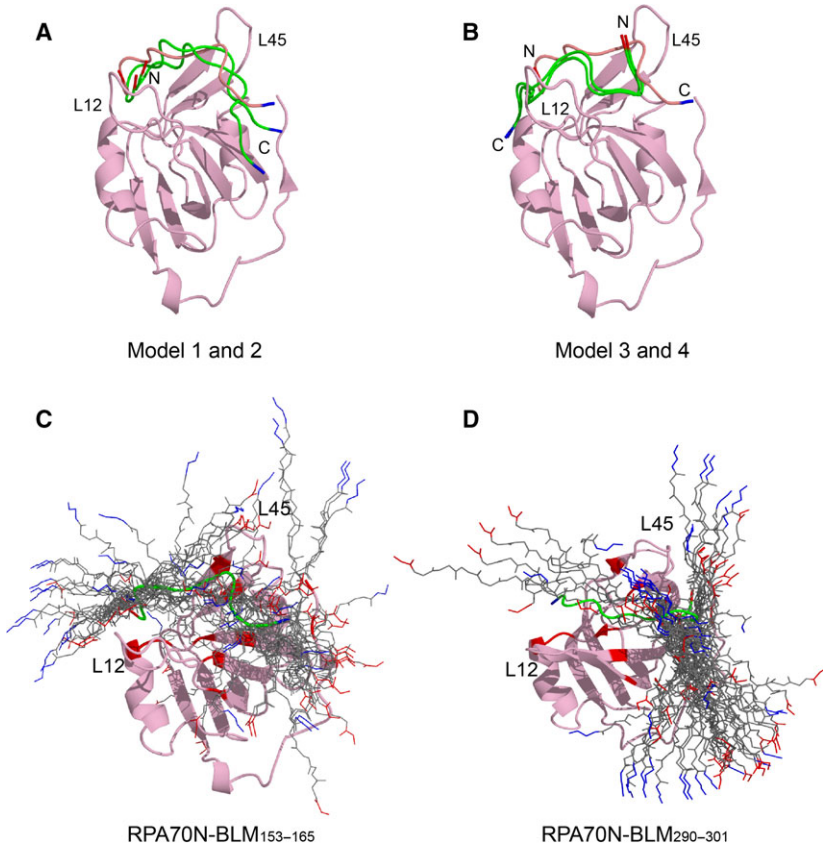

Fig. 7. (A,B) Docking models of RPA70N-$BLM_{153–165}$ complex. (A) Peptides of model 1 and 2 from HADDOCK (green) are the same orientation of model 1 peptide from CABS-dock (pink). (B) Peptides of model 3 and 4 from HADDOCK (green) have reverse orientations. (C,D) The 50 lowest energy docking models of (C) RPA70N-$BLM_{153–165}$ complex (D) RPA70N-$BLM_{290–301}$ complex by pep-ATTRACT server. Each model 1 peptide of CABS-dock is shown in green.

BLM (153–165)	DW D D M D D F D T S E T
BLM (290–301)	E F D D - D D Y D T D F V
ETAA1 (599–610)	TW E A - D D V D D D L L
ATRIP (54–65)	D F T A - D D L E E L D T

Fig. 8. Sequence alignment of $BLM_{153–165}$, $BLM_{290–301}$, $ETAA1_{599–610}$, and $ATRIP_{54–65}$. Hydrophobic residues are marked in red and acidic residues are marked in blue.

located in the position equivalent to F55 of ATRIP in its complex with RPA70N. This result suggests that the protein-protein interaction is not only mediated by electrostatic attraction but also by precisely tuned hydrophobic interactions. The negative charge and hydrophobicity of the BLM peptides are not localised within the peptide sequences. This could explain why both orientations of the RPA70N-bound peptides appeared in our docking simulations.

Because of the importance of these RPA-protein interactions in the damage response system, inhibitors have been developed for potential anticancer drugs [28,33–35]. We found that the K_ds of the BLM peptide–RPA70N complexes are similar to that of the ATRIP–RPA70N complex [20]. Furthermore, 3,3′,5,5′-tetraiodothyroacetic acid, which is a known competitor for the ATRIP binding site on RPA70N, can also inhibit the interaction of $BLM_{153–165}$ with RPA70N. These results suggest that protein interactions with RPA70N involve a common strategy and that the BLM-RPA interaction can be inhibited in the same way as other interactions.

Although the p53 peptide forms an amphipathic helix in the crystal structure of the p53/RPA70N complex [7], the BLM-RPA docking models suggest that the BLM peptides do not form secondary structures. CD spectroscopy showed that the BLM peptides do not possess secondary structure in solution and that RPA binding does not induce the peptides to form secondary structures (Fig. S2 and Doc. S1). The BLM peptides' conformation is closer to that of a linked ligand which simultaneously bound to 'site 1′ (near S55) and 'site 2' (near T60) in a previous study [34]. Our NMR data showed that both S55 and T60 experience prominent chemical shift perturbations upon binding to both BLM peptides. Furthermore, the docking models of the RPA70N-BLM complex support that the BLM peptides make contact with these

two locations of RPA70N. In contrast, the p53 peptide does not make contact with the 'site 2' region of RPA70N. This comparison gives insight into how RPA-mediated protein-protein interaction can be modulated depending on the contact area on RPA70N.

Unlike other RPA70N-binding proteins studied previously, the N-terminal region of BLM contains at least two RPA70N binding sites that have a similar μM K_d. However, although the RPA-binding affinities of the two BLM peptides that were used in this study are of the same order of magnitude, the RPA70N-$BLM_{153–165}$ had ~2-fold higher binding affinity than the RPA70N-$BLM_{290–301}$ complex. Although we chose each peptide based on its sequence homology with other RPA70N-binding peptides, there is a possibility that the peptide length could affect the binding affinity. However, if the binding affinity difference is inherent, we can develop hypotheses regarding the RPA-BLM interaction. First, more than one RPA molecule may be able to interact with a BLM molecule simultaneously, with a preference for the site with higher affinity. For example, an RPA70N molecule binds first to the $BLM_{153–165}$ site, and a second RPA molecule can interact with the $BLM_{290–301}$ site. Each RPA-binding site could interact independently or cooperatively. In this study, we examined each site as a separate peptide because BLM (153–301) and (150–340) constructs that contain both binding site were not expressed in *E.coli* to assess how the two sites play their roles in RPA binding, further studies are required. Second, the RPA-binding sites might be specific for the pathway that both proteins are involved in or dependent upon the expression levels of both proteins in the cell. Our understanding of the actual mechanism of BLM activation by RPA is incomplete, so further research on RPA-BLM binding *in vivo* is necessary.

In summary, we have studied the interaction of RPA70N with two BLM peptides by NMR spectroscopy and FPA. Two acidic peptides of BLM specifically bound to RPA70N with micromolar affinities. We found that RPA-BLM binding is mediated by interaction of acidic surface peptides of BLM with the basic cleft of RPA70N, similar to the binding modes of other RPA-interacting proteins. Our study confirms that the basic cleft region of RPA70N could be considered as a ubiquitous target for the inhibition of protein-protein interactions in cancer cells.

Acknowledgements

This work was supported by the National Research Foundation (NRF) of Korea (grant 2015R1C1A1A020 36725 to C-JP), which is funded by the Korean government (MSIT); by a GIST Research Institute grant funded by GIST in 2017; and by the Korea Basic Science Institute under R&D program (Project No.D37700) supervised by Ministry of Science and ICT, Korea. We thank Prof. Min-Gon Kim for providing access to the Cytation 5 instrument and Dr. Melissa Stauffer of Scientific Editing Solutions for editing the manuscript.

Author contributions

DK, SL, H-KC and C-JP designed the study. DK, SL prepared samples. DK, SL, K-SR, E-HK and C-JP planned and performed experiments. DK, SL, H-KC analysed the data. DK, SL and C-JP wrote the paper.

Data accessibility

Research data pertaining to this article is located at figshare.com: https://dx.doi.org/10.6084/m9.figshare.5821530.

References

1 He Z, Henricksen LA, Wold MS and Ingles CJ (1995) RPA involvement in the damage-recognition and incision steps of nucleotide excision repair. *Nature* **374**, 566–569.
2 Wold MS (1997) Replication protein A: a heterotrimeric, single-stranded DNA-binding protein required for eukaryotic DNA metabolism. *Annu Rev Biochem* **66**, 61–92.
3 Fanning E, Klimovich V and Nager AR (2006) A dynamic model for replication protein A (RPA) function in DNA processing pathways. *Nucleic Acids Res* **34**, 4126–4137.
4 Gomes XV and Wold MS (1996) Functional domains of the 70-kilodalton subunit of human replication protein A. *Biochemistry* **35**, 10558–10568.
5 Bochkarev A, Pfuetzner RA, Edwards AM and Frappier L (1997) Structure of the single-stranded-DNA-binding domain of replication protein A bound to DNA. *Nature* **385**, 176–181.
6 Xu X, Vaithiyalingam S, Glick GG, Mordes DA, Chazin WJ and Cortez D (2008) The basic cleft of RPA70N binds multiple checkpoint proteins, including RAD9, to regulate ATR signaling. *Mol Cell Biol* **28**, 7345–7353.
7 Bochkareva E, Kaustov L, Ayed A, Yi G-S, Lu Y, Pineda-Lucena A, Liao JCC, Okorokov AL, Milner J, Arrowsmith CH *et al.* (2005) Single-stranded DNA mimicry in the p53 transactivation domain interaction with replication protein A. *Proc Natl Acad Sci USA* **102**, 15412–15417.
8 Ning B, Feldkamp MD, Cortez D, Chazin WJ, Friedman KL and Fanning E (2015) Simian virus large

T antigen interacts with the N-terminal domain of the 70 kD subunit of replication protein A in the same mode as multiple DNA damage response factors. *PLoS One* **10**, e0116093.
9 Guler GD, Liu H, Vaithiyalingam S, Arnett DR, Kremmer E, Chazin WJ and Fanning E (2012) Human DNA helicase B (HDHB) binds to replication protein A and facilitates cellular recovery from replication stress. *J Biol Chem* **287**, 6469–6481.
10 Bass TE, Luzwick JW, Kavanaugh G, Carroll C, Dungrawala H, Glick GG, Feldkamp MD, Putney R, Chazin WJ and Cortez D (2016) ETAA1 acts at stalled replication forks to maintain genome integrity. *Nat Cell Biol* **18**, 1185–1195.
11 Croteau DL, Popuri V, Opresko PL and Bohr VA (2014) Human RecQ helicases in DNA repair, recombination, and replication. *Annu Rev Biochem* **83**, 519–552.
12 Bohr VA (2008) Rising from the RecQ-age: the role of human RecQ helicases in genome maintenance. *Trends Biochem Sci* **33**, 609–620.
13 Doherty KM, Sommers JA, Gray MD, Lee JW, von Kobbe C, Thoma NH, Kureekattil RP, Kenny MK and Brosh RMJ (2005) Physical and functional mapping of the replication protein A interaction domain of the Werner and Bloom syndrome helicases. *J Biol Chem* **280**, 29494–29505.
14 Brosh RM Jr, Li J-L, Kenny MK, Karow JK, Cooper MP, Kureekattil RP, Hickson ID and Bohr VA (2000) Replication protein A physically interacts with the Bloom's syndrome protein and stimulates its helicase activity. *J Biol Chem* **275**, 23500–23508.
15 Yodh JG, Stevens BC, Kanagaraj R, Janscak P and Ha T (2009) BLM helicase measures DNA unwound before switching strands and hRPA promotes unwinding reinitiation. *EMBO J* **28**, 405–416.
16 Hegnauer AM, Hustedt N, Shimada K, Pike BL, Vogel M, Amsler P, Rubin SM, van Leeuwen F, Guénolé A, van Attikum H *et al.* (2012) An N-terminal acidic region of Sgs1 interacts with Rpa70 and recruits Rad53 kinase to stalled forks. *EMBO J* **31**, 3768–3783.
17 Brosh RM Jr (2013) DNA helicases involved in DNA repair and their roles in cancer. *Nat Rev Cancer* **13**, 542–558.
18 Shen J-C, Lao Y, Kamath-Loeb A, Wold MS and Loeb LA (2003) The N-terminal domain of the large subunit of human replication protein A binds to Werner syndrome protein and stimulates helicase activity. *Mech Ageing Dev* **124**, 921–930.
19 Lee J-H, Park C-J, Arunkumar AI, Chazin WJ and Choi B-S (2003) NMR study on the interaction between RPA and DNA decamer containing cis-syn cyclobutane pyrimidine dimer in the presence of XPA: implication for damage verification and strand-specific dual incision in nucleotide excision repair. *Nucleic Acids Res* **31**, 4747–4754.
20 Souza-Fagundes EM, Frank AO, Feldkamp MD, Dorset DC, Chazin WJ, Rossanese OW, Olejniczak ET and Fesik SW (2012) A high-throughput fluorescence polarization anisotropy assay for the 70N domain of replication protein A. *Anal Biochem* **421**, 742–749.
21 Goddard TD and Kneller DG (2003) SPARKY 3. University of California, San Francisco, CA.
22 Bhattacharya S, Arunkumar AI, Sullivan SL, Botuyan M-V, Arrowsmith CH and Chazin WJ (2004) 1H, 13C and 15N assignments of single-stranded DNA binding domains from the 70 kDa subunit of human replication protein A. *J Biomol NMR* **82**, 195–196.
23 Lee S and Park C-J (2016) Backbone assignment of the N-terminal domain of human replication protein A 70 kDa. *J Korean Magn Reson Soc* **20**, 138–142.
24 Nikolovska-Coleska Z, Wang R, Fang X, Pan H, Tomita Y, Li P, Roller PP, Krajewski K, Saito NG, Stuckey JA *et al.* (2004) Development and optimization of a binding assay for the XIAP BIR3 domain using fluorescence polarization. *Anal Biochem* **332**, 261–273.
25 Kurcinski M, Jamroz M, Blaszczyk M, Kolinski A and Kmiecik S (2015) CABS-dock web server for the flexible docking of peptides to proteins without prior knowledge of the binding site. *Nucleic Acids Res* **43**, W419–W424.
26 Blaszczyk M, Kurcinski M, Kouza M, Wieteska L, Debinski A, Kolinski A and Kmiecik S (2016) Modeling of protein-peptide interactions using the CABS-dock web server for binding site search and flexible docking. *Methods* **93**, 72–83.
27 The PyMOL Molecular Graphics System, Version 1.8 Schrödinger, LLC.
28 Frank AO, Vangamudi B, Feldkamp MD, Souza-Fagundes EM, Luzwick JW, Cortez D, Olejniczak ET, Waterson AG, Rossanese OW, Chazin WJ *et al.* (2014) Discovery of a potent stapled helix peptide that binds to the 70N domain of replication protein A. *J Med Chem* **57**, 2455–2461.
29 van Zundert GCP, Rodrigues JPGLM, Trellet M, Schmitz C, Kastritis PL, Karaca E, Melquiond ASJ, van Dijk M, de Vries SJ and Bonvin AMJJ (2016) The HADDOCK2.2 web server: user-friendly integrative modeling of biomolecular complexes. *J Mol Biol* **428**, 720–725.
30 de Vries SJ, Rey J, Schindler CEM, Zacharias M and Tuffery P (2017) The pepATTRACT web server for blind, large-scale peptide-protein docking. *Nucleic Acids Res* **45**, W361–W364.
31 Arunkumar AI, Stauffer ME, Bochkareva E, Bochkarev A and Chazin WJ (2003) Independent and coordinated functions of replication protein A tandem high affinity single-stranded DNA binding domains. *J Biol Chem* **278**, 41077–41082.
32 Stauffer ME and Chazin WJ (2004) Physical interaction between replication protein A and Rad51 promotes

exchange on single-stranded DNA. *J Biol Chem* **279**, 25638–25645.

33 Feldkamp MD, Frank AO, Kennedy JP, Patrone JD, Vangamudi B, Waterson AG, Fesik SW and Chazin WJ (2013) Surface reengineering of RPA70N enables co-crystallization with an inhibitor of the RPA interaction motif of ATRIP. *Biochemistry* **52**, 6515–6524.

34 Frank AO, Feldkamp MD, Kennedy JP, Waterson AG, Pelz NF, Patrone JD, Vangamudi B, Camper DV, Rossanese OW, Chazin WJ *et al.* (2013) Discovery of a potent inhibitor of replication protein A protein-protein interactions using a fragment linking approach. *J Med Chem* **56**, 9242–9250.

35 Patrone JD, Pelz NF, Bates BS, Souza-Fagundes EM, Vangamudi B, Camper DV, Kuznetsov AG, Browning CF, Feldkamp MD, Frank AO *et al.* (2016) Identification and optimization of anthranilic acid-based Inhibitors of replication protein A. *ChemMedChem* **11**, 893–899.

36 Dolinsky TJ, Nielsen JE, McCammon JA and Baker NA (2004) PDB2PQR: An automated pipeline for the setup of Poisson-Boltzmann electrostatics calculations. *Nucleic Acids Res* **32**, 665–667.

Supporting information

Additional Supporting Information may be found online in the supporting information tab for this article:

Fig. S1. (A) Simultaneous display of $BLM_{290–301}$ (cyan) on the RPA70N-$BLM_{153–165}$ complex. (B) Interactions per residue of BLM peptides with RPA70N.

Fig. S2. CD spectra of the BLM peptides, RPA70N, and RPA70N-BLM complexes.

Table S1. Details of structural clustering for the RPA70N-$BLM_{153–165}$ complex.

Table S2. Details of structural clustering for the RPA70N-$BLM_{290–301}$ complex.

Table S3. Details of Structural Clustering for RPA70N-$p53_{33–60}$ complex.

Table S4. Cluster statistics of RPA70N-$BLM_{153–165}$ complex (HADDOCK simulation).

Doc. S1. Supplementary method.